Microfluid Nanofluid (2011) 10:749–759
DOI 10.1007/s10404-010-0706-0

RESEARCH PAPER

Chaotic mixing using source–sink microfluidic flows in a PDMS chip

H. Cumhur Tekin · Venkataragavalu Sivagnanam · A. Tuna Ciftlik · Abdeljalil Sayah · Caroline Vandevyver · Martin A. M. Gijs

Received: 8 June 2010 / Accepted: 6 September 2010 / Published online: 16 October 2010

Abstract We present an active fixed-volume mixer based on the creation of multiple source–sink microfluidic flows in a polydimethylsiloxane (PDMS) chip without the need of external or internal pumps. To do so, four different pressure-controlled actuation chambers are arranged on top of the 5 µl volume of the mixing chamber. After the mixing volume is sealed/fixed by microfluidic valves made using 'microplumbing technology', a virtual source–sink pair is created by pressurizing one of the membranes and, at the same time, releasing the pressure of a neighboring one. The pressurized air deforms the thin membrane between the mixing and control chambers and creates microfluidic flows from the squeezed region (source) to the released region (sink) where the PDMS membrane is turned into the initial state. Several schemes of operation of virtual source–sink pairs are studied. In the optimized protocol, mixing is realized in just a sub-second time interval, thanks to the implementation of chaotic advection.

Keywords Fixed-volume mixer · Valve · Chaotic advection · Source–sink flow · PDMS · Microfluidics

Electronic supplementary material The online version of this article (doi:10.1007/s10404-010-0706-0) contains supplementary material, which is available to authorized users.

H. C. Tekin (✉) · V. Sivagnanam · A. T. Ciftlik · A. Sayah · M. A. M. Gijs
Laboratory of Microsystems, Ecole Polytechnique Fédérale de Lausanne, 1015 Lausanne, Switzerland
e-mail: huseyincumhur.tekin@epfl.ch

C. Vandevyver
Research Commission SNF, Ecole Polytechnique Fédérale de Lausanne, 1015 Lausanne, Switzerland

1 Introduction

Mixing is one of the crucial steps of biological analysis protocols in microfluidic devices. The flow inside microchannels generally has a low Reynolds number, defined by $Re = U_0 h/\nu < 100$, where U_0 is the average flow speed, $h \sim 100$ µm the typical cross-sectional dimension of the microchannel (e.g., channel height), and ν the kinematic viscosity of the fluid. Mixing is naturally dominated by a slow diffusion process, with a characteristic time that is given by $t_{\mathrm{mix}} = l_{\mathrm{st}}^2/D$, where l_{st} is the striation length over which diffusion needs to take place for mixing, and D is the diffusion coefficient. Due to the typical size of D, also the Péclet number is large ($Pe = U_0 w_c/D > 100$) in a microfluidic cell or channel of width w_c. Several passive and active mixers were realized using microfluidic chip technology, mainly by shrinking the striation length (Nguyen and Wu 2005; deMello 2006). Hydrodynamic focusing (Knight et al. 1998), lamination (Kamholz et al. 1999; Cieslicki and Piechna 2009), and chaotic advection (Stroock et al. 2002; Xia et al. 2005) are major principles in passive mixers that do not need any external force other than the flow itself to create mixing. Most passive mixers are designed for a certain range of Reynolds number (Re) and Péclet number (Pe) associated with the fluid flow in the microfluidic channel. On the other hand, active mixers provide enhanced control potential and independence of the flow parameters by using external forces to create perturbed flow (Nguyen and Wu 2005). Such mixers offer to users a flexible device for 'on-demand' mixing (Lu et al. 2002). Most importantly, active mixers offer fluid metering when using fixed-volume mixing chambers (Urbanski et al. 2006), so that precise quantities of reagents can be dosed. The planar laminar mixer (Evans et al. 1997) is one of the early examples of an active fixed-volume mixer. Here, mixing was created by two source–sink pairs, where

there was a periodic removal of fluid from a mixing reservoir by a sink and a re-injection into the reservoir from a source. With only a few liquid removal–injection cycles, complete mixing was obtained in this powerful device based on chaotic advection (Aref 1984). However, high-cost micromachining techniques were used to realize the mixer in a composite silicon-quartz chip with integrated bubble valves and pumps to create pulsed source–sink flows (Jones and Aref 1988; Evans et al. 1997). Several other actuation methods were introduced in fixed-volume mixers, based on either acoustic (Rife et al. 2000; Yang et al. 2001; Jang et al. 2007), electrokinetic (Chang et al. 2008; Harnett et al. 2008) or magnetic (Yuen et al. 2003; Agarwal et al. 2005) principles, which require either certain electrochemical properties of fluids or expensive microfabrication and integration techniques. Magnetic beads manipulation (Rida and Gijs 2004) was also used for mixing in fixed volumes (Grumann et al. 2005). Although mixing was generated by simply changing the magnetic force in time, magnetic beads were needed within the reagents, necessitating extra fluidic steps in the protocol and also possibly inducing unwanted aspecific adsorption of rare molecules on the bead surfaces.

'Microplumbing technology' has been presented as an extremely interesting concept that enables valving, pumping, and mixing functionalities in affordable polydimethylsiloxane (PDMS) chips for parallel batch processing of biological samples (Hong et al. 2004). These devices were fabricated by the soft lithography technique and were composed of two distinct elastomer layers, called the control and fluidic layers (Unger et al. 2000). By pressurizing the control layer, the deflection of a thin membrane between the layers blocks the fluidic flow inside a fluidic channel with half-circular cross-section, thereby implementing a valving functionality. Valves were the basic building blocks of this technology, and pumping could be realized by periodic actuation of three valves in series. A rotary mixer was realized by pumping the fluid inside a ring-shaped chamber (Chou et al. 2001). It was shown that perfect mixing for a 15 nl volume was achieved in 30 s, which is 170-fold faster than pure diffusion-based mixing (Chou et al. 2001). In this fixed-volume mixer, the striation length was decreased algebraically in time using shear forces (Squires and Quake 2005) that relatively long mixing time and channels were required to get efficient mixing even for nanoliter scale. This situation can pose a bottle neck for applications using higher (microliter) sample volumes, such as for clinical diagnosis (Nagrath et al. 2007; Gijs et al. 2010), rare molecule detection (Herrmann et al. 2007; Sivagnanam et al. 2009), and DNA microarraying (Yuen et al. 2003). On the other hand, in chaotic advection, the distance between fluidic streams is reduced by a constant factor with each mixing cycle, which involves exponential stretching and folding of the fluidic streams (Aref 1984). In the staggered herringbone mixer, which is one of the most performant chaotic passive mixers for continuous flow systems, after N mixing cycles, the striation length is decreased to $l_{st} = h/2^N$ (Stroock et al. 2002; Squires and Quake 2005). Mixing is completed when the time to diffuse over a striation length l_{st}^2/D is comparable to the cycle time $t_{cyc} = N \cdot L_{cyc}/U_0$, where L_{cyc} is the geometrical length needed to perform one stretching-folding cycle (Squires and Quake 2005). The required time for complete mixing is derived and experimentally validated as being proportional to $(L_{cyc}/U_0) \cdot \ln(Pe) \sim \ln(Pe)/Pe$ in the chaotic mixer (Jones 1991; Stroock et al. 2002; Squires and Quake 2005). Therefore, continuous flow chaotic advection mixers are characterized by a fast mixing performance for high flow rates (large Pe). It was also confirmed in the staggered herringbone mixer that mixing was completed for a flow with $Pe = 10^5$ in only 1.5 s, i.e., 670-fold faster than pure diffusion-based mixing (Stroock et al. 2002).

In this paper, we present a new active fixed-volume chaotic mixing concept, based on multiple source–sink microfluidic flows without need of external or internal pumps and implemented using PDMS 'microplumbing technology'. To do so, four mixer control chambers are implemented on top of a simple rectangular-like mixing chamber and are actuated by pressurized air. A virtual source–sink pair is generated by pressurizing one control chamber, while depressurizing the neighboring one. The pressurized air deforms the thin membrane between the mixing and control chambers and creates fluidic flows from the squeezed region (source) to the released region (sink) where the PDMS membrane is turned into the initial state. With a periodic operation of source–sink pairs, extremely fast mixing can be established by chaotic advection within the closed chamber. Several protocols of operation of source–sink pairs are studied. In the optimized device, perfect mixing is achieved in only a sub-second time interval ($\sim$350 ms, i.e., 7000-fold faster than the pure diffusion-based mixing) for a compact 5 µl mixing volume.

2 Materials and methods

2.1 Materials

GM 1075 SU-8 negative photoresist was purchased from Gersteltec Sàrl (Pully, Switzerland). Propylene glycol methyl ether acetate (PGMEA) 99% SU-8 developer was obtained from Sigma-Aldrich Chemie GmbH (Buchs, Switzerland). PDMS Sylgard 184 was acquired from Dow Corning GmbH (Wiesbaden, Germany). 4 inch silicon (Si) test wafers and de-ionized water (DIW) were taken from the Center of Micro-Nano-Technology (EPFL, Lausanne, Switzerland). E122 red-colored and E141 green-colored

solutions diluted in distilled water were purchased from Coop (Lausanne, Switzerland). 1 ml borosilicate H-TLL-PE syringes were bought from ILS Innovative Labor Systeme GmbH (Stutzerbach, Germany). MHP1 normally closed 3/2 way solenoid valves were obtained from Festo SA (Yverdon-les-Bains, Switzerland). Micro-line ethyl vinyl acetate tubes with 0.51 mm inner diameter were taken from Fisher Scientific (Wohlen, Switzerland).

2.2 Design

The microfluidic device contains a mixing chamber, four valves and corresponding control chambers. In Fig. 1a, the device has the mixing chamber and control chamber channels filled with red- and green-colored solutions, respectively. The three-dimensional device is composed of four distinct PDMS layers, like schematically shown in Fig. 1b. The bottom and top layers are 2.5 mm thick to give mechanical stability to the structure, while the middle layers have 160 and 110 μm thickness to implement a thin PDMS membrane between control and fluidic channels. Valving and mixing functionalities are realized by actuating thin PDMS membranes with the applied pressure from control chamber access ports (shown in Fig. 1a). Valves are used for the isolation of the mixing chamber so that a fixed volume is preserved while creating pressure in the mixer control chambers. A 50 μm-thick disc-shaped PDMS membrane with 750 μm radius is realized between the valve control chamber and the fluidic channels for valving (PDMS layer 2 in Fig. 1b). By pressurizing the valve control chamber, the thin membrane is deformed and it blocks the connection via having a 100 μm radius and realized in PDMS layer 3. Even during low pressure actuation, a perfect leakage-free valve can be obtained.

As the design in Fig. 1c shows, four rectangular mixer control chambers with a width 1500 μm and a length 4000 μm are placed on top of the 5 μl rectangular-like mixing chamber with 250 μm depth. Everywhere, a 110 μm thick PDMS membrane, called a mixer control chamber membrane, is formed between the mixing and the mixer control chambers. As described in Fig. 1d, releasing the mixer control chamber pressure and, at the same time, pressurizing another mixer control chamber induces an unidirectional flow, as if a source and a sink are applied in the squeezed and released region, respectively. We call these two control chambers generating a flow a "virtual source–sink pair" (VSSP); the sequential mixer control chamber membrane actuation avoids the need of external or internal pumps connected to the fixed-volume fluidic chamber (Evans et al. 1997; McQuain et al. 2004).

In the proposed device, after closing all inlet and outlet valves (shown in Fig. 1a), mixing is realized with multiple

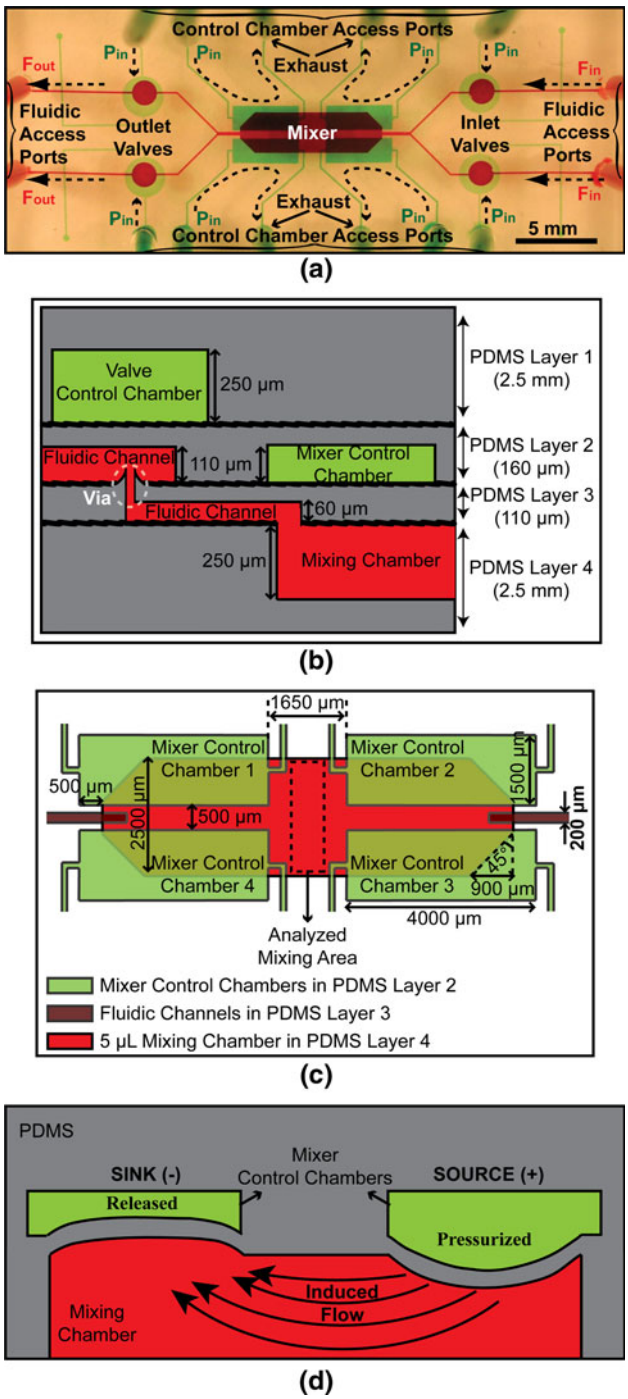

Fig. 1 **a** Photograph of the final PDMS chip with the control circuit comprising four leakage-free valves, and a microfluidic mixing chamber with connecting microchannels that are filled with different colored solutions. F_{in}, F_{out}, and P_{in} are referred to fluidic inlet, fluidic outlet, and pressure inlet, respectively, and *dashed lines with arrow heads* indicate the corresponding fluidic or pressurized air flow direction. **b** Cross-sectional schematic view showing the four bonded PDMS layers. **c** Geometrical parameters of the microfluidic mixing chamber with the four mixer control chambers. **d** Illustration of virtual source–sink pair flow generation inside the microfluidic mixing chamber. Actuation of one mixer control chamber, while releasing at the same time the previously pressurized mixer control chamber, induces the flow

VSSPs, created by actuating the mixer control chamber membranes at a defined sequence. A pulsed source–sink flow results in a confirmed chaotic advection mixing process in a bounded-plane domain (Stremler et al. 2004). However, in a mixing domain, chaos can coexist with regular regions where fluidic stretching is only linear in time (Hertzsch et al. 2007). Fluids inside the regular regions do not interact with the rest of the domain (except by diffusion) and hinder fast mixing (Ottino and Wiggins 2004). If a particle is trapped in these regular regions, it circulates on a closed path in each mixing cycle and turns to near the same initial position. It was shown that streamlines of different source–sink pairs should be transversal and also the forming shear should be strong and monotonic (i.e., acting in the same direction) to break down the closed paths and make the particle increasingly fall far away from the original point (Hertzsch et al. 2007; Beuf et al. 2010). Therefore, the source–sink pairs should be engineered precisely to reduce the importance of the regular regions. In this paper, eight different mixing configurations using the four mixer control chambers are proposed and analyzed experimentally. As described in Fig. 2, the mixing methods are grouped into four categories, labeled as no-pair, where source and sink are operated individually, two-VSSP, three-VSSP and four-VSSP configurations. Each configuration is composed of a number of periodic strokes creating flows in the mixing chamber and expressed as a letter 's' followed by a number defining the sequence in the mixing cycle and a '+' or '−' sign, indicating a source (pressurized membrane) or a sink (released membrane) function, respectively. During operation, PDMS membranes preserve their previous status until a fresh stroke pressurizes or releases them.

2.3 Microfabrication

SU-8 micropatterns fabricated on 4 inch silicon wafers by standard photolithography are used as a mold to replicate the PDMS layers. First, the wafers are treated in oxygen plasma at 500 W for 7 min and subsequently spin-coated with GM1075 SU-8 negative photoresist. After the soft-bake step at 130°C, the resist layer is exposed, and then the post-exposure baking step is conducted at 100°C. The resist is developed in PGMEA 99% and the mold micropatterns are revealed on the Si wafer. 2-layer SU-8 processing is performed to generate a mold for realizing the microfluidic vias (Kartalov et al. 2006). To do so, after the post-exposure step of the 60 μm thick first SU-8 layer, a second SU-8 layer with 160 μm thickness is processed on top and the development of the two layers is done together. A scanning electron microscopy (SEM) image of the final 2-layer SU-8 mold is shown in Fig. S1 of the Supplementary Material. In total, four distinct PDMS layers are realized by pouring liquid 10:1 PDMS Sylgard 184 mixture on the molds. PDMS is spun at 750 and 1000 rpm for 20 s to obtain the 160 μm-thick PDMS layer 2 and the 110 μm-thick PDMS layer 3. The layers are cured for 1 h at 100°C and bonded together to create a monolithic device in a three-step assembly process. To create irreversible sealing between PDMS layers (Duffy et al. 1998), the contact surfaces are activated using an O_2 plasma at 12 W for 40 s before each sealing step. It is hard to handle thin PDMS membranes

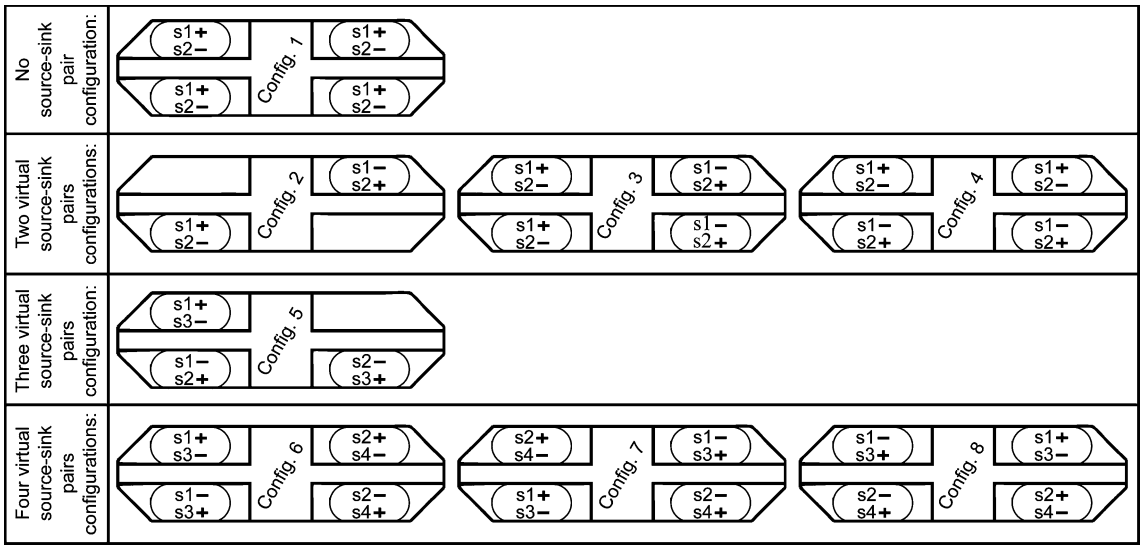

Fig. 2 The eight different active mixing configurations studied, defined by changing the sequence of actuation of the four mixer control chambers creating virtual source–sink pairs in different order. The character '*s*' on top of a pair of control chambers indicates the pressurized source (expressed as '+') or depressurized sink (expressed as '−'), respectively, at a particular sequence of the mixing cycle (expressed by the number 1, 2, 3 or 4)

without any support, which is the reason why the second and third layers are bonded with the others while still present on their mold. After the bonding step of PDMS layer 1 and 2, the access ports of fluidic and control layers are punched using a dispensing needle with 1.37 mm inner diameter (H. Sigrist + Partner, Matzingen, Switzerland).

2.4 Experimental setup

The experimental setup for mixing in the microfluidic device is illustrated in Fig. 3. Two syringes are mounted on a Nemesys dosing system (Cetoni GmbH, Korbußen, Germany) and are connected to the fluidic inlets of the device with elastic tubes. The flow rates of the syringes are set with the Nemesys software. The valve control chambers are filled with DIW to eliminate bubble creation originating from continuous gas diffusion through the thin PDMS membrane (Metref et al. 2007) into the fluidic channel due to the steady pressurized air. On the other hand, the mixer control chambers that are connected also to the exhaust ports do not need to be filled with DIW, since the thin mixer control chamber membrane is not exposed to the steady pressurized air. The precisely adjusted compressed air is obtained with a MS6-LRP-1/4-D4-A8 pressure regulator (Festo SA, Yverdon-les-Bains, Switzerland) and applied through elastic tubes to the control chamber access ports of the device under the control of solenoid valves. To power the solenoid valves, electrical signals are commanded by a in house-developed C-program on a computer and supplied through a FPGA-based development board (FPGA4U acquired from IC/EPFL, Lausanne, Switzerland), which is equipped with a driving circuitry to supply high current levels. +5 V are applied to solenoid valves to pressurize the microfluidic valves on-chip. Square waveform electrical signals having +5 V maximum and 0 V minimum in different phases with a 50% duty cycle power the four solenoid valves to generate pulsed actuation of the four mixer control chambers at a certain frequency (1–20 Hz). The phase difference between the electrical signals applied to the solenoid valves to provide consecutive pressurized sources on mixer control chambers (shown in Fig. 2) is set to be $2\pi/N_{vssp}$, where N_{vssp} is the number of VSSP in the mixing strategies.

2.5 Mixing characterization

For mixing characterization, spreading of E122 red-colored molecules with a 2×10^{-6} cm^2 s^{-1} diffusion coefficient (Claux and Vittori 2007) is studied in the fluidic chamber during the various mixing strategies. E122 molecules give more robust measurements than fluorescent molecules avoiding the influence of the photobleaching effect (Orhan et al. 2008). To do the analysis, two syringes are filled with DIW and red-colored distilled water solution, respectively. Then, the red-colored solution (E122) and the DIW are side-by-side introduced at 100 nl s^{-1} flow rates to the mixing chamber from the fluidic inlets (shown in Fig. 3). After closing all inlet and outlet valves to seal the mixing

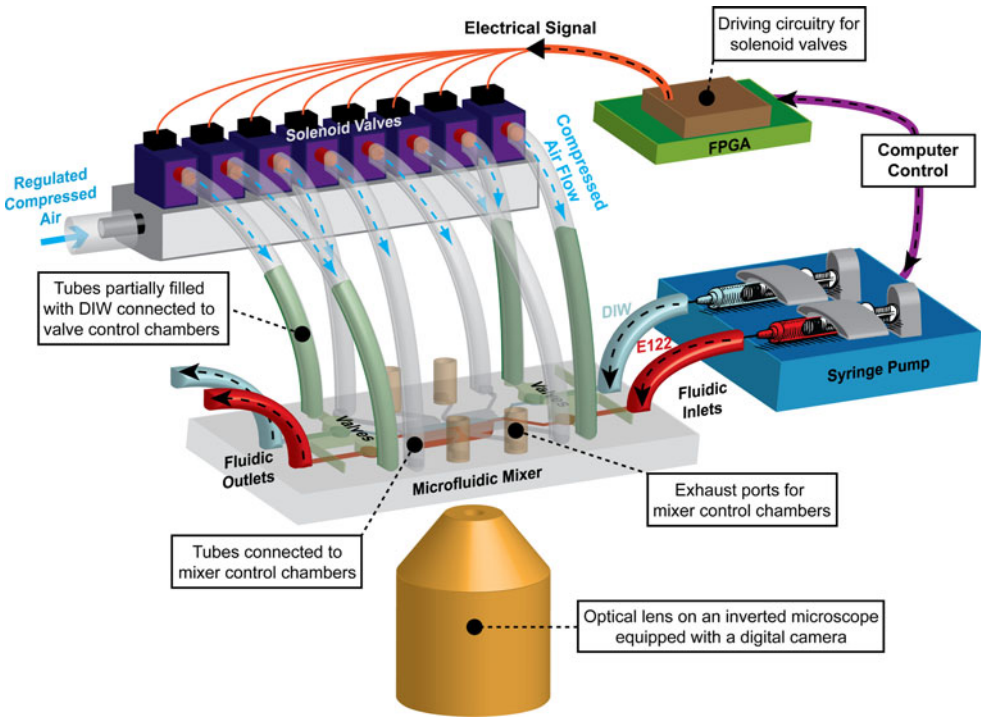

Fig. 3 Illustration of the experimental setup for mixing characterization. After the fluids (de-ionized water (DIW) and E122 colored solution) are introduced side-by-side to the microfluidic device by a syringe pump, microfluidic valves are pressurized to seal the mixing chamber and mixing is started by actuating solenoids valves controlled through a FPGA board. The optical micrographs characterizing the mixing are captured by an inverted microscope equipped with a digital camera

chamber, mixing is started. Before and during mixing operations, optical micrographs are taken using a monochrome digital camera (Pixelink PL-B741U) with a TV adapter 0.5× (Zeiss 456101) mounted on an inverted microscope (Zeiss Axio Observer A1) having a 2.5× optical lens (Zeiss EC-Plan NEOFLUAR).

The mixing performance is characterized by analyzing the intensity profiles of the chamber from the obtained images using an in house-developed MATLAB program. For the analysis, micrographs are converted to negative gray images, with the maximum intensity achieved on the red-colored part. We analyze the center mixing area that is uncovered by the control chambers (shown in Fig. 1c) to avoid the influence of unsteady intensity profiles under the actuated PDMS membrane surfaces during the mixing operation. The studied region covers the most important part of the mixing area with dimensions of ~2450 × 811 μm corresponding to 441 × 146 pixels. The analyzed region is adequate to observe the mixing characteristics, since it has a central position for all possible regular regions with respect to the pulsed source–sink pairs (Raynal et al. 2004; Hertzsch et al. 2007). To quantify the mixing, a mixing index (MI) corresponding to the image intensities is calculated using the following expression (Lu et al. 2002):

$$\mathrm{MI}(t) = \sqrt{\frac{1}{N}\sum_{k:1}^{N}\left(\frac{I(t,k) - I_{\mathrm{avg}}(t)}{I_{\mathrm{avg}}(t)}\right)^2}, \quad (1)$$

where N is the total pixel number, $I(t,k)$ is the intensity of the pixel 'k' and $I_{\mathrm{avg}}(t)$ is the average intensity value of the pixels in the inspected area at a time 't'. This mixing index is a measure of the standard deviation of the image intensity profile and it approaches zero when uniformity of the concentration is reached across the chamber.

To allow calculation of the instantaneous Reynolds and Péclet numbers, one should know the flow speed U_0 inside the mixing chamber, which is obtained as follows. A deformed mixer control chamber membrane creates an instantaneous volume displacement of the liquid during collapsing. To measure the displaced volume (ΔV), the mixing chamber is filled with DIW and then all valves are closed except one valve. By pressurizing the mixer control chamber, liquid moves through the open valve and fills the connecting microfluidic channel that has well-defined dimensions, so that the displaced volume can be easily quantified under the inverted microscope. The closure time of the membrane (Δt), the time required for totally collapsing the membrane with an applied pressure, is also measured with the Pixelink high frame rate camera. U_0 is calculated from these measured values on the cross-sectional area of the membrane halve perimeter (the shaded area shown in Fig. S2 of the Supplementary Material), through which the displaced volume is spread as:

$$|U_0| = \frac{\Delta V}{\Delta t}\cdot\frac{1}{(w_{\mathrm{m}} + l)\cdot h}, \quad (2)$$

with $w_{\mathrm{m}} = 1000$ μm and $l = 3500$ μm the width and length of the mixer control chamber membrane, respectively, and $h = 250$ μm the height of the mixing chamber.

3 Experimental results and discussion

3.1 Valve

The proposed 3-layer valve structure is realized using the same operational principle as Beebe's valve (Beebe et al. 2000), but air instead of pH responsive hydrogel drives our valve to obtain a faster response time. Within a wide range of applied pressures to the valve control chamber, the disc-shaped valving membrane is deflected and it efficiently blocks the colored solution, as shown in Fig. 4. The deformed membrane needs to close only the small fluidic connection hole (via) between fluidic layers for valving and hence a 15 kPa actuation pressure is more than sufficient to get a perfect leakage-free valve, avoiding the need of a very thin PDMS membrane (~10 μm), like in a 2-layer soft lithography valve (Studer et al. 2004). Our valve structures are fabricated using SU-8 molds (Lorenz et al. 1997), which gives us the freedom of using high aspect-ratio microfluidic channels. On the contrary, due to the fact that the cross-linked SU-8 is a thermosetting polymer (Chen et al. 2006), it is impossible to obtain hemispherical micropatterns as a mold for 2-layer valves, as enabled by using a resist reflow method (Unger et al. 2000).

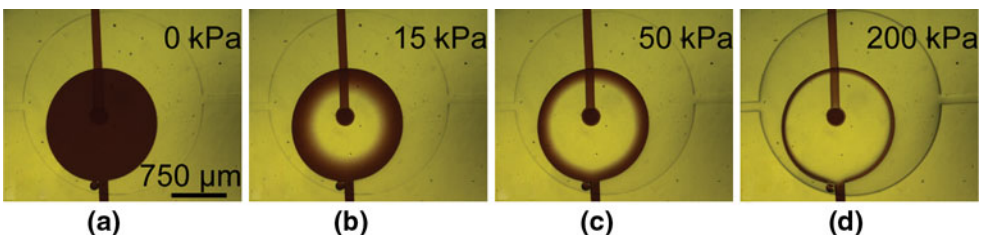

Fig. 4 Optical micrographs of **a** an open valve and **b–d** closed valves using an actuation pressure of 15, 50, and 200 kPa, respectively

3.2 Mixer performance: qualitative

After the mixing chamber is filled with parallel laminar flow streams of red E122 colored solution and DIW, the inlet and outlet valves are closed, and the mixing is performed. When using pure diffusion-based mixing without using any actuation, mixing times of the order of 30 min are needed, as shown in the upper panel row of Fig. 5. Sequential photographs of the mixing operation for different active mixing strategies using a 70 kPa actuation of the mixer control chambers at 10 Hz are shown in the bottom panel rows of Fig. 5. In active mixing configuration 1, where all membranes are actuated at the same time, there is nearly no color alteration appearing in the chamber. While creating two VSSPs in the mixing channel, like in mixing configuration 2–4, only small liquid perturbations are observed but they are not really adequate for fast mixing. In these configurations, positions of source and sink are interchanged in each stroke, during which the flow direction is changed without affecting the streamline profile in the chamber. Therefore, liquids are shuffled between actuation regions on the same streamlines, resulting in a diffusion-dominated mixing process. Three VSSPs are used in mixing configuration 5. During mixing, a single vortex rotating in a counter-clockwise direction is created in half of the chamber by simply locating the source–sink pairs in a triangular geometry, as already explained in Fig. 2. The center of this vortex is altered in each source–sink flow stroke, but the vortex cannot circulate in the whole chamber volume. Hence, in large remaining regions in the mixing chamber, mixing is realized by a slow diffusion process. Although configuration 5 gives better results than the mixing configuration with two VSSPs, it is not an optimized solution for an efficient mixing in the entire domain.

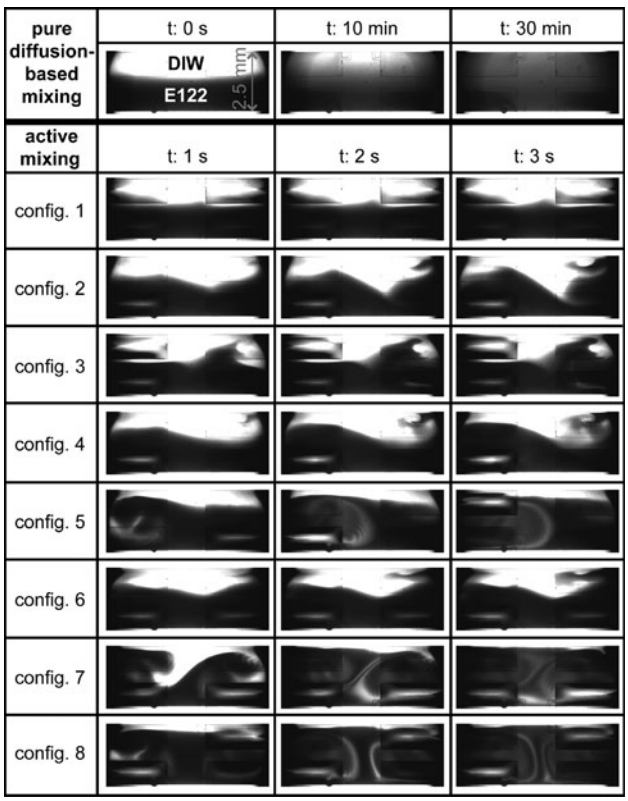

Fig. 5 Sequential optical micrographs of the mixing of a colored solution and color-less de-ionized water when using either pure diffusion-based mixing, or the eight different active mixing strategies studied using a 70 kPa actuation pressure at 10 Hz

Four-VSSP configurations (configurations 6, 7, and 8) are also examined in Fig. 5. The mixing performance using configuration 6 becomes worse than the three-VSSP case. Flows generated by consecutive source–sink pairs are widely separated and almost do not affect each other in configuration 6; fluid is trapped on a same streamline profile like in a two-VSSP configuration and the mixing is governed mainly by a slow diffusion process. On the other hand, color homogeneity is obtained in a matter of a few seconds when using mixing configuration 7 or 8, as shown in the two lower panel rows of Fig. 5. The slow-motion video clip of the mixing process with configuration 8 is also supplied in Movie 1 of the Supplementary Material. Two co-rotating and counter-rotating vortices are generated in mixing configuration 7 and 8, respectively. Figure 6a shows in more detail the experimental observations obtained for configuration 7 and 8 during the second stroke (s2) and fourth stroke (s4) of the fifteenth mixing cycle ($\sim$1.5 s) with mixer control chamber actuation at 70 kPa and 10 Hz. For both mixing configurations, the induced vortices change their centers periodically, as schematically indicated in Fig. 6a, which is in favor of a fast mixing process (Sturman and Wiggins 2009).

3.3 Mixer performance: quantitative

We study in more detail now mixing configurations 7 and 8, which have suggested the best mixing performances. For efficient pulsed source–sink flow mixing, the fluid in the chamber should behave as a chaotic sea where exponential stretching and folding of fluids is observed (Cola et al. 2006). However, regular regions, where fluidic stretching is linear in time, exhibit only slow diffusion-based mixing (Raynal et al. 2004; Hertzsch et al. 2007). To examine mixing configuration 7 and 8, streamline simulations of the generated flows for stroke 1 and 2 are conducted using the finite element method (COMSOL Multiphysics 3.5a) by solving the Navier–Stokes equations for incompressible flows in the three-dimensional domain of a rigid mixing chamber:

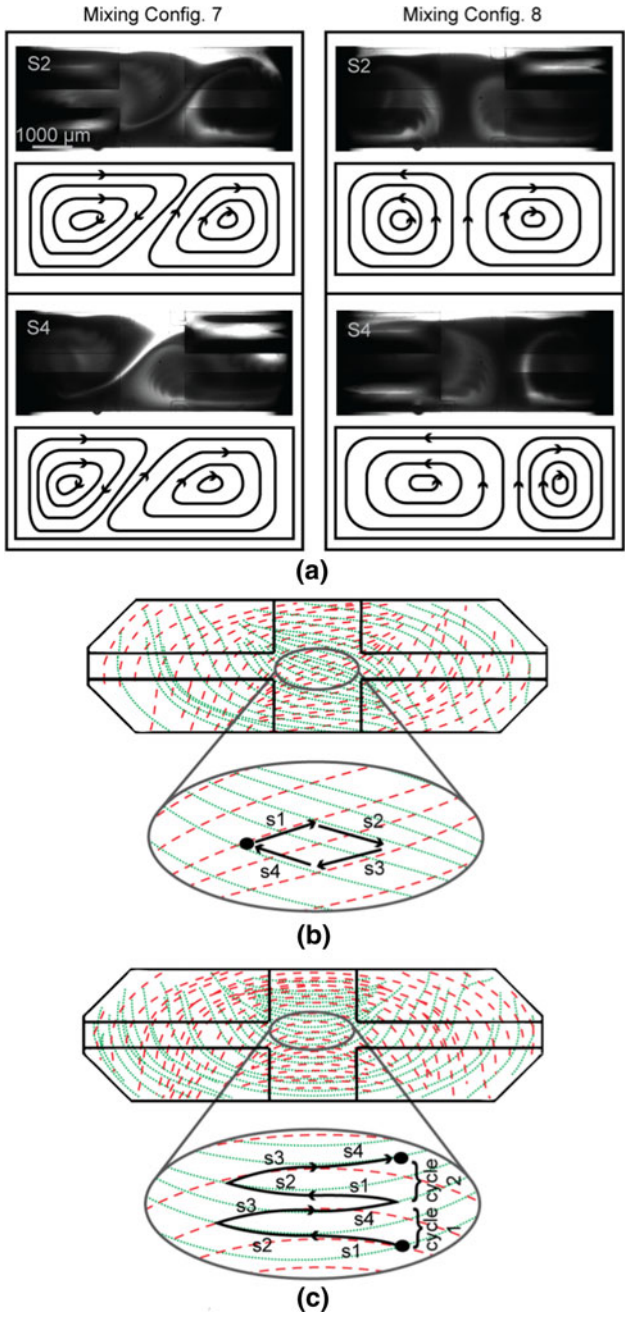

Fig. 6 **a** Optical photographs and schematic flow patterns of mixing configuration 7 and 8 during the second (*s2*) and forth (*s4*) strokes of the fifteenth mixing cycle with control chamber actuations at 70 kPa and 10 Hz. Either two co-rotating or two counter-rotating vortices, whose centers are altered in each stroke, are generated with configuration 7 and 8, respectively. **b**, **c** Streamline profiles of mixing configuration 7 and 8, respectively, obtained from simulations using COMSOL Multiphysics 3.5a. Stroke 1 (*s1*), drawn in dashed lines, shares the same streamline profile as stroke 3 (*s3*); stroke 2 (*s2*), drawn in dotted lines, shares the same streamline profile as stroke 4 (*s4*). The ellipses in **b**, **c** are zooms on the center of the mixing chamber, to illustrate the trajectory of a liquid volume element during subsequent strokes of the mixing process

$$\rho\frac{\partial \mathbf{u}(t)}{\partial t} + \rho(\mathbf{u}\cdot\nabla\mathbf{u}) = -\nabla p + \eta\nabla^2\mathbf{u} \qquad \nabla\cdot\mathbf{u} = 0 \tag{3}$$

where $\mathbf{u}$ is the fluid velocity, and ρ and η are the density and viscosity of the fluid. The streamline profiles for stroke 3 and 4 are similar to those of stroke 1 and 2, respectively. As boundary conditions for the steady-state analysis, the volume displacement generated during a mixer control chamber membrane deflection is modeled as a volume flow that is perpendicular to and uniformly distributed over the actuated mixer control chamber membrane area; this flow can be either an inlet for a source function, or an outlet for a sink function. When following an infinitesimal liquid volume element during four consecutive strokes in configuration 7, fluid at the center of the chamber moves on a kind of a closed loop inside a regular region, as suggested in Fig. 6b. Since streamlines of different source–sink pairs are transversal and also the forming shear is monotonic at the center of the mixing chamber for configuration 8, the liquid volume element changes abruptly the sign of its momentum after each pair of strokes, as suggested in Fig. 6c, resembling the folding flow patterns as found in the chaotic staggered herringbone mixer (Stroock et al. 2002). When the volume element reaches the lower part of the mixing chamber, it will be transported upwards again by the two vortices (see Fig. 6a) without entering a regular region. Hence, much faster mixing is expected with configuration 8 than with configuration 7, based on the streamline profile analysis (Hertzsch et al. 2007). In order to verify the mixing quantitatively, MI values for both configurations are examined for different actuation pressures at 10 Hz. Figure 7a and b shows the MI values obtained from the image analysis for configuration 7 and 8, respectively, at different times of the mixing process. The fast oscillatory behavior of MI, which is superposed to the decreasing trend line, is a consequence of the mixer control membrane actuation at 10 Hz that directly affects the intensity of the colored solution (Hardy et al. 2009). This oscillatory behavior is more pronounced in configuration 7 that it is characterized by an up-and-down oscillatory flow in the detection area at the center of the mixing chamber, as schematically shown in Fig. 6b. From the MI values of Fig. 7a and b, we observe that the fastest mixing performance is achieved for the highest actuation pressures that evidently give rise to the highest flow velocities (highest *Pe* value) in the mixing chamber. Mixing configuration 8 is clearly better performing than configuration 7. When we define $T_{0.1}$ as the time required to reach a MI value of 0.1, which is a common criterion for quantifying adequate mixing (Mao et al. 2010), we can plot the $T_{0.1}$ values for

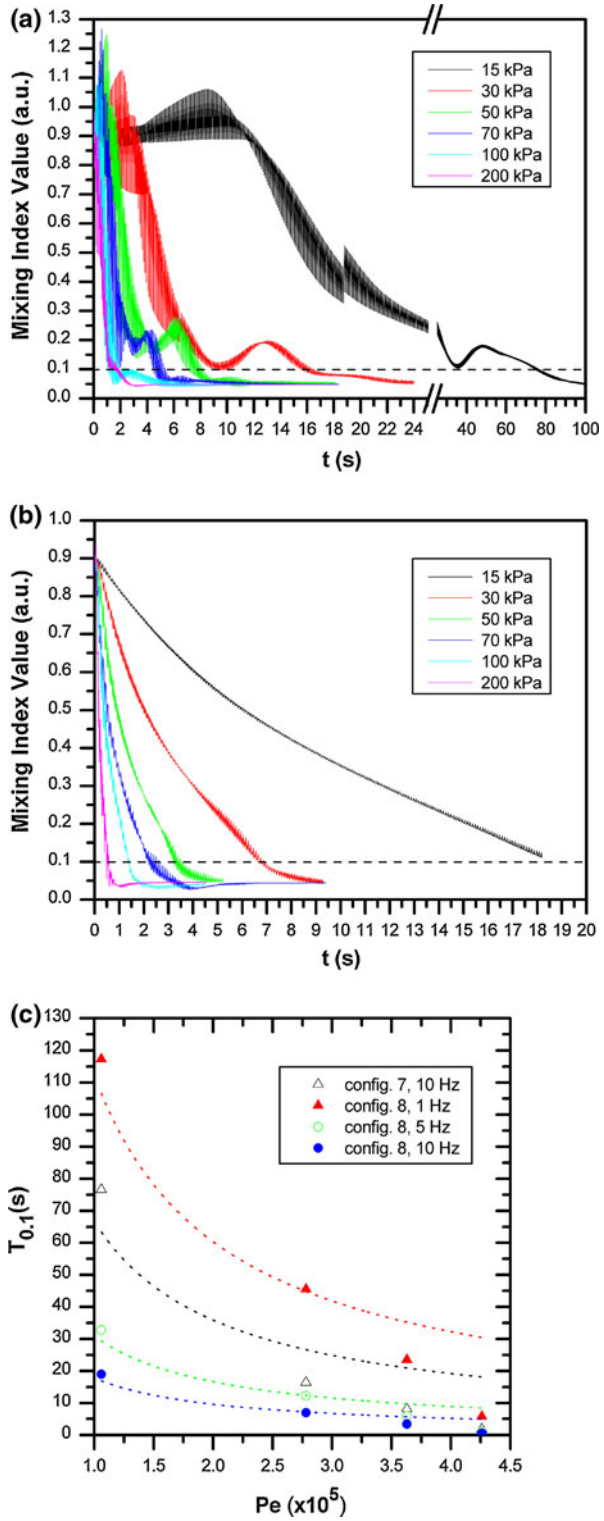

Fig. 7 **a**, **b** MI values, experimentally obtained from image analysis, at different times of the mixing process for configuration 7 and configuration 8, respectively, using different actuation pressures at 10 Hz. **c** Experimental mixing times $T_{0.1}$, derived from graphs of the type of **a**, **b**, as a function of the Péclet number for mixing configuration 7 with 10 Hz actuation, and for mixing configuration 8 with 1, 5, and 10 Hz actuation frequencies. The dotted lines are $T_{0.1} \sim \ln(Pe)/Pe$ fits based on chaotic advection theory

Table 1 Displaced volume in the mixing chamber with a width $w_c = 2500$ μm and corresponding Péclet number of the induced flow due to actuation of a single PDMS membrane with different control chamber pressures

Actuation pressure (kPa)	Displaced volume (nl)	*Pe*
15	141	1.06×10^5
30	241	2.78×10^5
50	365	3.63×10^5
70	468	4.02×10^5
100	531	4.12×10^5
200	573	4.26×10^5

different actuation frequencies as a function of *Pe*. The latter were calculated, taking into account the experimentally observed 15 ms closure time of a single PDMS actuation membrane, and using the geometrical parameters illustrated in Fig. S2 of the Supplementary Material; the *Pe* values are also listed in Table 1.

The experimental data curves of Fig. 7c show the dependence of $T_{0.1}$ on *Pe*, for a 10 Hz actuation frequency using mixing configuration 7, and for 1, 5, and 10 Hz actuation frequencies using configuration 8. The dotted curves are fits to a $\ln(Pe)/Pe$ dependence, in line with mixing based on chaotic advection (Squires and Quake 2005; Mao et al. 2010). The $T_{0.1}$–*Pe* curves corresponding to configuration 8 with 5 and 10 Hz actuations can be well fitted. This is clearly not the case when using a 10 Hz actuation frequency in mixing configuration 7. In the latter, a liquid volume element in the detection area does not have the momentum sign changes after each pair of strokes, as is typical for the chaotic advection-dominated configuration 8 indeed. One also notes that the $T_{0.1}$–*Pe* curve corresponding to the use of a 1 Hz actuation frequency in configuration 8 is not well fitted by the $\ln(Pe)/Pe$ function, which can be understood as follows. In each stroke, a source–sink flow is induced during the 15 ms closure time of the actuation membrane, followed by a waiting time equal to the half actuation period minus the closure time. For example, for a 1 Hz actuation frequency, the waiting time is 485 ms, considerably higher than the closure time. In this case, mixing is dominated by a diffusion process rather than by the stretching and folding of fluid streams.

Finally, we want to highlight the excellent performance of our mixing configuration 8 for the higher actuation frequencies. Figure 8 shows a sequence of images and corresponding MI values obtained during mixing using configuration 8 with an actuation pressure of 200 kPa and an actuation frequency of 20 Hz (the maximum operation frequency of the solenoid valves), compared with the MI values of pure diffusion-based mixing. It shows a mixing time $T_{0.1}$ of configuration 8 to be only 350 ms, which is ~7000-fold faster than the pure diffusion-based mixing

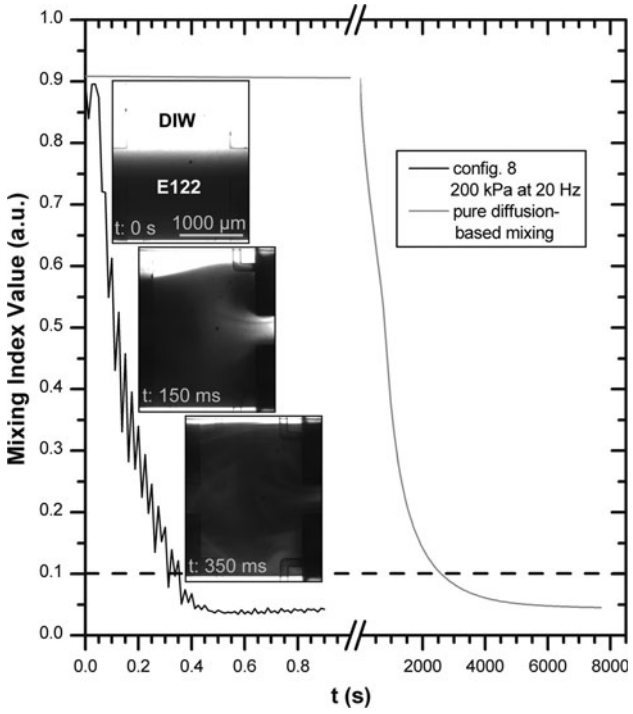

Fig. 8 Optical photographs of three different sequences of the mixing process and corresponding MI values for configuration 8 using 200 kPa actuation pressure at 20 Hz, compared with the MI values of pure diffusion-based mixing. The mixing time $T_{0.1}$ for configuration 8 is only 350 ms, while it is 2500 s in pure diffusion-based mixing

time. This is, to our knowledge, the fastest mixing yet reported for fixed microliter volumes. Since each membrane becomes source and sink in a mixing cycle, at least two periods of membrane closure time (Δt) are needed in a mixing cycle in order to completely collapsing and then releasing a control membrane. If not, a membrane will only displace a partial volume underneath and the mixing time will be increased due to the decrease in flow velocity. One can increase the actuation frequency up to $\sim$30 Hz and still have complete deflection of a membrane. Mixer control chambers can be driven also with high pressures up to 500 kPa, the maximum pressure compatible with PDMS–PDMS bonding (Eddings et al. 2008). However, an increase in actuation pressure beyond 200 kPa will only slightly decrease the mixing time, since the liquid displacement due to a single membrane actuation and so the flow velocity saturate at 200 kPa, as suggested in Table 1.

4 Conclusion

We presented a novel mixing concept based on multiple source–sink flows in microfluidic chips that were realized using PDMS 'microplumbing technology'. Several protocols of operation of source–sink pairs were studied. In the optimized device, perfect mixing was achieved in only a sub-second time interval for a compact 5 µl mixing volumes. This excellent performance was achieved thanks to the implementation of chaotic advection, characterized by stretching and folding of the microfluidic streams. The use of SU-8 molds for replication of the PDMS chips allowed easy prototyping and provided design freedom, for example for choosing the aspect-ratio of the microfluidic chambers and channels. Also, the performance of the valves was not critically dependent on actuation pressure, the degree of hemisphericity of the channels or membrane thickness, giving rise to a robust technology. We therefore think that the proposed mixer will offer new opportunities for integrated, low-cost, fast and high-volume biological analysis applications.

Acknowledgments We would like to thank Meng Shen of the Laboratory of Microsystems of EPFL (Switzerland) and Dr. Bo Song of the Laboratory of Lanthanide Supramolecular Chemistry of EPFL for helpful discussions and suggestions, Di Jiang of the Laboratory of Microsystems of EPFL (Switzerland) for solving programming issues on the FPGA board and the staff of the EPFL Center of MicroNano Technology (CMI) for assistance in the chip fabrication issues.

References

Agarwal AK, Sridharamurthy SS, Beebe DJ, Jiang HR (2005) Programmable autonomous micromixers and micropumps. J Microelectromech Syst 14(6):1409–1421. doi:10.1109/Jmems.2005.859101

Aref H (1984) Stirring by chaotic advection. J Fluid Mech 143(June):1–21

Beebe DJ, Moore JS, Bauer JM, Yu Q, Liu RH, Devadoss C, Jo BH (2000) Functional hydrogel structures for autonomous flow control inside microfluidic channels. Nature 404(6778):588–590

Beuf A, Gence JN, Carriere P, Raynal F (2010) Chaotic mixing efficiency in different geometries of hele-shaw cells. Int J Heat Mass Transf 53(4):684–693. doi:10.1016/j.ijheatmasstransfer.2009.10.024

Chang ST, Beaumont E, Petsev DN, Velev OD (2008) Remotely powered distributed microfluidic pumps and mixers based on miniature diodes. Lab Chip 8(1):117–124. doi:10.1039/B712108c

Chen JK, Ko FH, Chan CH, Huang CF, Chang FC (2006) Using imprinting technology to fabricate three-dimensional devices from moulds of thermosetting polymer patterns. Semicond Sci Technol 21(9):1213–1220. doi:10.1088/0268-1242/21/9/001

Chou H-P, Unger MA, Quake SR (2001) A microfabricated rotary pump. Biomed Microdevices 3(4):323–330

Cieslicki K, Piechna A (2009) Investigations of mixing process in microfluidic manifold designed according to biomimetic rule. Lab Chip 9(5):726–732. doi:10.1039/B811005k

Claux B, Vittori O (2007) Bismuth film electrode as an alternative for mercury electrodes: determination of azo dyes and application for detection in food stuffs. Electroanalysis 19(21):2243–2246. doi:10.1002/elan.200703978

Cola BA, Schaffer DK, Fisher TS, Stremler MA (2006) A pulsed source–sink fluid mixing device. J Microelectromech Syst 15(1):259–266. doi:10.1109/Jmems.2005.863786

deMello AJ (2006) Control and detection of chemical reactions in microfluidic systems. Nature 442(7101):394–402. doi:10.1038/Nature05062

Duffy DC, McDonald JC, Schueller OJA, Whitesides GM (1998) Rapid prototyping of microfluidic systems in poly(dimethylsiloxane). Anal Chem 70(23):4974–4984

Eddings MA, Johnson MA, Gale BK (2008) Determining the optimal pdms-pdms bonding technique for microfluidic devices. J Micromech Microeng 18(6). doi:10.1088/0960-1317/18/6/067001

Evans J, Liepmann D, Pisano AP (1997) Planar laminar mixer. Proc IEEE MEMS Workshop, pp 96–101

Gijs MAM, Lacharme F, Lehmann U (2010) Microfluidic applications of magnetic particles for biological analysis and catalysis. Chem Rev 110(3):1518–1563. doi:10.1021/Cr9001929

Grumann M, Geipel A, Riegger L, Zengerle R, Ducree J (2005) Batch-mode mixing on centrifugal microfluidic platforms. Lab Chip 5(5):560–565. doi:10.1039/B418253g

Hardy BS, Uechi K, Zhen J, Kavehpour HP (2009) The deformation of flexible pdms microchannels under a pressure driven flow. Lab Chip 9(7):935–938. doi:10.1039/B813061b

Harnett CK, Templeton J, Dunphy-Guzman KA, Senousy YM, Kanouff MP (2008) Model based design of a microfluidic mixer driven by induced charge electroosmosis. Lab Chip 8(4):565–572. doi:10.1039/B717416k

Herrmann M, Roy E, Veres T, Tabrizian M (2007) Microfluidic elisa on non-passivated pdms chip using magnetic bead transfer inside dual networks of channels. Lab Chip 7(11):1546–1552. doi:10.1039/B707883h

Hertzsch JM, Sturman R, Wiggins S (2007) DNA microarrays: design principles for maximizing ergodic, chaotic mixing. Small 3(2):202–218. doi:10.1002/smll.200600361

Hong JW, Studer V, Hang G, Anderson WF, Quake SR (2004) A nanoliter-scale nucleic acid processor with parallel architecture. Nat Biotechnol 22(4):435–439. doi:10.1038/Nbt951

Jang LS, Chao SH, Holl MR, Meldrum DR (2007) Resonant mode-hopping micromixing. Sens Actuators A 138(1):179–186. doi:10.1016/j.sna.2007.04.052

Jones SW (1991) The enhancement of mixing by chaotic advection. Phys Fluids A 3(5):1081–1086

Jones SW, Aref H (1988) Chaotic advection in pulsed-source sink systems. Phys Fluids 31(3):469–485

Kamholz AE, Weigl BH, Finlayson BA, Yager P (1999) Quantitative analysis of molecular interaction in a microfluidic channel: the t-sensor. Anal Chem 71(23):5340–5347

Kartalov EP, Walker C, Taylor CR, Anderson WF, Scherer A (2006) Microfluidic vias enable nested bioarrays and autoregulatory devices in newtonian fluids. Proc Natl Acad Sci USA 103(33):12280–12284. doi:10.1073/pnas.0602890103

Knight JB, Vishwanath A, Brody JP, Austin RH (1998) Hydrodynamic focusing on a silicon chip: mixing nanoliters in microseconds. Phys Rev Lett 80(17):3863–3866

Lorenz H, Despont M, Fahrni N, LaBianca N, Renaud P, Vettiger P (1997) Su-8: a low-cost negative resist for mems. J Micromech Microeng 7(3):121–124

Lu LH, Ryu KS, Liu C (2002) A magnetic microstirrer and array for microfluidic mixing. J Microelectromech Syst 11(5):462–469. doi:10.1109/Jmems.2002.802899

Mao XL, Juluri BK, Lapsley MI, Stratton ZS, Huang TJ (2010) Milliseconds microfluidic chaotic bubble mixer. Microfluid Nanofluidics 8(1):139–144. doi:10.1007/s10404-009-0496-4

McQuain MK, Seale K, Peek J, Fisher TS, Levy S, Stremler MA, Haselton FR (2004) Chaotic mixer improves microarray hybridization. Anal Biochem 325(2):215–226. doi:10.1016/J.Ab.2003.10.032

Metref L, Herrera F, Berdat D, Gijs MAM (2007) Contactless electrochemical actuator for microfluidic dosing. J Microelectromech Syst 16(4):885–892. doi:10.1109/Jmems.2007.892893

Nagrath S, Sequist LV, Maheswaran S, Bell DW, Irimia D, Ulkus L, Smith MR, Kwak EL, Digumarthy S, Muzikansky A, Ryan P, Balis UJ, Tompkins RG, Haber DA, Toner M (2007) Isolation of rare circulating tumour cells in cancer patients by microchip technology. Nature 450(7173):1235–1239. doi:10.1038/Nature06385

Nguyen NT, Wu ZG (2005) Micromixers—a review. J Micromech Microeng 15(2):R1–R16. doi:10.1088/0960-1317/15/2/R01

Orhan JB, Parashar VK, Flueckiger J, Gijs MAM (2008) Internal modification of poly(dimethylsiloxane) microchannels with a borosilicate glass coating. Langmuir 24(16):9154–9161. doi:10.1021/La801317x

Ottino JM, Wiggins S (2004) Introduction: mixing in microfluidics. Philos Trans R Soc Lond A 362(1818):923–935. doi:10.1098/rsta.2003.1355

Raynal F, Plaza F, Beuf A, Carriere P, Souteyrand E, Martin JR, Cloarec JP, Cabrera M (2004) Study of a chaotic mixing system for DNA chip hybridization chambers. Phys Fluids 16(9):L63–L66. doi:10.1063/1.1775807

Rida A, Gijs MAM (2004) Manipulation of self-assembled structures of magnetic beads for microfluidic mixing and assaying. Anal Chem 76(21):6239–6246. doi:10.1021/Ac049415j

Rife JC, Bell MI, Horwitz JS, Kabler MN, Auyeung RCY, Kim WJ (2000) Miniature valveless ultrasonic pumps and mixers. Sens Actuators A 86(1–2):135–140

Sivagnanam V, Song B, Vandevyver C, Gijs MAM (2009) On-chip immunoassay using electrostatic assembly of streptavidin-coated bead micropatterns. Anal Chem 81(15):6509–6515. doi:10.1021/Ac9009319

Squires TM, Quake SR (2005) Microfluidics: fluid physics at the nanoliter scale. Rev Mod Phys 77(3):977–1026

Stremler MA, Haselton FR, Aref H (2004) Designing for chaos: applications of chaotic advection at the microscale. Philos Trans R Soc Lond A 362(1818):1019–1036. doi:10.1098/rsta.2003.1360

Stroock AD, Dertinger SKW, Ajdari A, Mezic I, Stone HA, Whitesides GM (2002) Chaotic mixer for microchannels. Science 295(5555):647–651

Studer V, Hang G, Pandolfi A, Ortiz M, Anderson WF, Quake SR (2004) Scaling properties of a low-actuation pressure microfluidic valve. J Appl Phys 95(1):393–398. doi:10.1063/1.1629781

Sturman R, Wiggins S (2009) Eulerian indicators for predicting and optimizing mixing quality. New J Phys 11. doi:10.1088/1367-2630/11/7/075031

Unger MA, Chou HP, Thorsen T, Scherer A, Quake SR (2000) Monolithic microfabricated valves and pumps by multilayer soft lithography. Science 288(5463):113–116

Urbanski JP, Thies W, Rhodes C, Amarasinghe S, Thorsen T (2006) Digital microfluidics using soft lithography. Lab Chip 6(1):96–104. doi:10.1039/B510127a

Xia HM, Wan SYM, Shu C, Chew YT (2005) Chaotic micromixers using two-layer crossing channels to exhibit fast mixing at low Reynolds numbers. Lab Chip 5(7):748–755. doi:10.1039/B502031j

Yang Z, Matsumoto S, Goto H, Matsumoto M, Maeda R (2001) Ultrasonic micromixer for microfluidic systems. Sens Actuators A 93(3):266–272

Yuen PK, Li GS, Bao YJ, Muller UR (2003) Microfluidic devices for fluidic circulation and mixing improve hybridization signal intensity on DNA arrays. Lab Chip 3(1):46–50. doi:10.1039/B210274a